Journal of Materials Chemistry A

Accepted Manuscript

ROYAL SOCIETY OF CHEMISTRY

www.rsc.org/materialsA

Journal Name

ARTICLE

A Facile preparation of $CoFe_2O_4$ nanoparticles on Polyaniline-Functioned Carbon Nanotubes as Enhanced Catalysts for Oxygen Evolution Reaction

Received 00th January 20xx,
Accepted 00th January 20xx

DOI: 10.1039/x0xx00000x

www.rsc.org/

Yang Liu,[ab] Jing Li,[ab] Feng Li,[ab] Wenzhu Li,[ab] Haidong Yang,[ab] Xueyao Zhang,[ab] Yansheng Liu[ab] and Jiantai Ma*[ab]

Designing and preparing high efficient non-precious metal electrocatalyst for the oxygen evolution reaction (OER) is extremely urgent but still remains a challenge. In this study, a polyaniline-multiwalled carbon nanotubes (PANI-MWCNTs) supported, high performance $CoFe_2O_4$ nanoparticles (NPs) loading electrocatalyst ($CoFe_2O_4$/PANI-MWCNTs) is synthesized through a novel and simple in-situ process at modest condition. It is found that the introduction of PANI improves the synergistic effect between $CoFe_2O_4$ NPs and MWCNTs, so as to promote the electrical conductivity and stability of the catalyst. Meanwhile, PANI provides more active sites to attach $CoFe_2O_4$ NPs uniformly and tightly. By electrochemical measurement, the electrocatalyst displays excellent OER activities at a low overpotential of 314 mV for 10 mA cm^{-2} current density and a small Tafel slope 30.69 mV dec^{-1} in 1 M KOH at a scan rate of 5 mV s^{-1}. Furthermore, this electrocatalyst exhibits remarkably long durability evaluated by continuously cycling 1000 cycles and stably working at 0.54 V (vs. Ag/AgCl) for at least 40 h. The achieved results confirm that $CoFe_2O_4$/PANI-MWCNTs hybrid is an earth-abundant and cheap fabricated anode material for OER.

Introduction

With gradual depletion of non-renewable energy resources, renewable energy resources now attract widely attention [1]. Hydrogen (H_2), as an important renewable energy resource, can be obtained by water splitting which is considered as an effective and environmentally friendly method [2, 3]. The water splitting reaction is composed of two half reactions: the oxygen evolution reaction (OER, $4OH^- \rightarrow 2H_2O + 4e^- + O_2$ in base) and the hydrogen evolution reaction (HER, $2H^+ + 2e^- \rightarrow H_2$ in acid) [4, 5]. However, the efficiency of H_2 production from water splitting is subject to the OER because of the sluggish kinetics of the OER at the anode [6, 7]. Thus, an efficient catalyst is needed to promote the 4-electron oxidation process and make OER proceed at low overpotential to lower the water splitting reaction energy barrier [8]. The oxides such as ruthenium (IrO_2) and iridium (RuO_2) are known to be the most active electrocatalysts for the OER owing to the low overpotential and small Tafel slope [9, 10]. However, the high cost and scarcity of IrO_2 and RuO_2 hinder the widespread commercialization of fuel cells and metal-air batteries [11, 12].

As is well-known, mixed transition metal oxides with spinel structure, due to their diverse advantages such as strong super paramagnetic property, good biocompatibility, high electronic conductivity, abundant resources, low cost and environmental friendliness, have attracted much attention [13-15]. Therefore, numerous kinds of transition oxide catalysts can be used as superior OER electrocatalysts, such as Co_3O_4/N-doped graphene hybrid [16], Co–Fe–O/rGO [17], $Ni_xCo_{3-x}O_4$ [18], Ni-Fe oxide [19] and $M_xMn_{3-x}O_4$ (M=divalent metals) [20]. Among the transition metal oxides, the spinel-type compounds with the general formula of AB_2X_4 (A, B=metal, X=chalcogen) have been shown as promising electrocatalysts for the OER [21, 22]. Li et al. [23] have reported that MFe_2O_4 (M = Co, Ni, Cu, Mn, etc.) nanofibers (NFs) synthesized by electrospinning and subsequent thermal treatment processes exhibited considerable catalytic activities for both OER and H_2O_2 reduction/detection in alkaline media. Meanwhile, $CoFe_2O_4$ NFs have shown the highest catalytic activities among the MFe_2O_4 NFs. Bian et al. [24] and Liu et al. [25] have also demonstrated the superior electrocatalytic activities of $CoFe_2O_4$ metarials for the OER and Oxygen Reduction Reaction (ORR).

Multiwalled carbon nanotubes (MWCNTs) are ideal electrocatalyst support owing to their high accessible surface area, good electronic conductivity and chemical stability [26, 27]. However, both size and high distributions of metal nanoparticles (NPs) directly deposited on MWCNTs are usually

[a] State Key Laboratory of Applied Organic Chemistry (SKLAOC), College of Chemistry and Chemical Engineering, Lanzhou University, Lanzhou 730000, PR China. E-mail: majiantai@lzu.edu.cn; Fax: +86-931-8912582; Tel: +86-931-8912577
[b] Gansu Provincial Engineering Laboratory for Chemical Catalysis, College of Chemistry and Chemical Engineering, Lanzhou University, Lanzhou 730000,PR China.

† Footnotes relating to the title and/or authors should appear here.
Electronic Supplementary Information (ESI) available: [details of any supplementary information available should be included here]. See DOI: 10.1039/x0xx00000x

not uniform to ascribe to their inert surface. Wrapping carbon nanotubes with conducting polymers is a good way to solve this

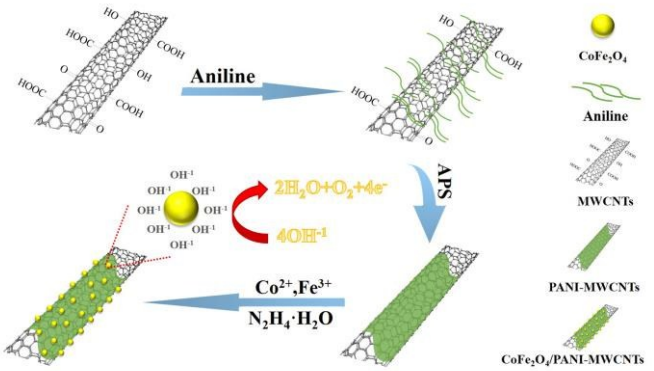

Scheme 1: The process for the preparation of the $CoFe_2O_4$/PANI-MWCNTs and application in the oxygen evolution reaction.

issue [28]. Among conducting polymers, polyaniline (PANI) is one of the most widely studied conducting polymers on account of its unique π-conjugated structures, which lead to good environmental stability and unique redox properties [27, 29, 30]. Moreover, PANI has numerous amino groups as anchor sites for metal ions, preventing metal NPs from aggregating [31].

Spinel-type oxides are usually synthesized through solid-state method, hydrothermal technique, co-precipitation, micro-emulsion route and sol-gel process [32-35]. And in general, these traditional methods need grinding or firing the mixtures of the corresponding metal precursors, which call for elevated temperature and prolonged time to overcome the reaction energy barriers. Therefore, it remains challenging to synthesize homogenous and ultrasmall nanocrystalline spinels under facile conditions. In this work, a novel and simple in-situ method has been reported to prepare monodisperse $CoFe_2O_4$ NPs on the PANI-covered multiwalled carbon nanotubes ($CoFe_2O_4$/PANI-MWCNTs) at mild temperature and room atmosphere. The synthesis of the procedure is illustrated in Scheme 1. The aniline monomer was firstly selectively adsorbed onto the carbon surface via preferential π–π conjugation between the aniline and acid-treatment MWCNTs surface and then polymerized in situ on the carbon surface via ammonium peroxodisulfate (APS) and $FeSO_4$ oxidation in acidic solution [28,30]. Subsequently, the aqueous solution containing a fixed ratio of 2:1 Fe^{3+}/Co^{2+} precursors and hydrazine hydrate was heated at 120°C for 4 hours to obtain $CoFe_2O_4$ NPs. The as-synthesized $CoFe_2O_4$/PANI-MWCNTs hybrid performed remarkable catalytic activity and long-term stability towards OER in alkaline solution, exceeding $CoFe_2O_4$ NPs and $CoFe_2O_4$/MWCNTs hybrid. The results further demonstrated PANI in this hybrid played a crucial role in mediated functionalization. It not only improved the catalytic performance for the OER, but also led to homogeneous distribution of $CoFe_2O_4$ NPs.

Experimental

Materials

Multi-walled carbon nanotubes were purchased from Shenzhen Nanotech Port Co. Ltd, sulfuric acid (95%~98% w/w), nitric acid (65%~68% w/w), Aniline (≥99.5% w/w), hydrogen chloride (36%~38% w/w), ammonium peroxydisulfate ($(NH_4)_2S_2O_8$, ≥98% w/w), iron (II) sulfate heptahydrate ($FeSO_4 \cdot 7H_2O$, ≥99% w/w), Iron (III) chloride hexahydrate ($FeCl_3 \cdot 6H_2O$, ≥99% w/w), Cobalt (II) nitrate hexahydrate ($CoN_2O_6 \cdot 6H_2O$, ≥99% w/w), Ruthenium(IV) oxide (99.95% metal basis), Iridium(IV) oxide (99.9% metal basis), Hydrazine monohydrate (≥80% w/w), deionized water (18.2 MΩ cm) were commercially available and used throughout the experiments. All the commercialized chemicals used in this study were of analytical grade and not further purified.

Acid-treatment of MWCNTs

The MWCNTs were treated with an acid mixture in the presence of sonication for their functionalization. Specifically, 200 mg MWCNTs were mixed in a 500 mL round bottle flask with 150 mL HNO_3 and 50ml H_2SO_4 (3:1(v/v)) at 75 °C for 4 h. After reaction, the obtained black powder was separated by suction filtration and washed with deionized water until its pH value became approximately 7 before drying at 70 °C.

Preparation of PANI-MWCNTs

The PANI-MWCNTs were prepared by the in-situ polymerization of aniline in the presence of a carbon nanotube suspension [28, 36]. To synthesize the PANI-MWCNTs composite (e.g., aniline monomer: MWCNTs = 1:20 (w:w)), 100 mg acid-treatment MWCNTs and 10 mL of 2 M HCl aqueous solution was sonicated at room temperature for about an hour and then mixed with 5 μL aniline monomer to sonicate for another half an hour. 5 mL of 2 M HCl aqueous solution containing 100 mg $(NH_4)_2S_2O_8$ and 5 mg $FeSO_4 \cdot 7H_2O$ which served as the oxidant was later added dropwise with vigorous stirring. The reaction mixture was constantly stirred in an ice bath (< 5 °C) for 1 h and then reacted at room temperature for 3 h. The products were purified by centrifugation with ethanol and deionized water and then dried in vacuum freezing dryer to constant weight (101 mg, 96.2%). PANI-MWCNTs composites with weight ratios of 1:1, 1:2, 1:5, 1:10, 1:35, 1:50 (w:w) were also prepared by the similar method. The product amounts and yield of PANI-MWCNTs composites were provided in Table S1.

Preparation of $CoFe_2O_4$/PANI-MWCNTs$_{1:20}$ (40 wt.%) composites

The PANI-MWCNT$_{1:20}$ (10 mg) was suspended in 10 mL of EtOH/H_2O (1:1, *v:v*) with ultrasonic treatment for 30 min to form a homogeneous solution. After sonication, designated amounts of $FeCl_3 \cdot 6H_2O$ (15.34 mg) and $CoN_2O_6 \cdot 6H_2O$ (8.26 mg) with 2:1 molar ratio were added to the above solution and the mixed solution was sonicated for another 10 min. Then, 20 mL of hydrazine hydrate were added to the mixture and stirred for half an hour. Afterwards, the above mixture was heating at 120 °C for 4 h. The product (14.7 mg, 88.0%) was collected by centrifugation and washed with deionized water and ethanol,

and then dried at 50 °C for 12 h. Other composites with different $CoFe_2O_4$ loading amounts (20 wt.%, 30 wt.%, 50 wt.%, 60 wt.%) and without support were also prepared with the same procedure. The product amounts and yield of $CoFe_2O_4$/PANI-MWCNTs$_{1:20}$ were shown in Table S2.

Characterization

The morphologies and microstructures of $CoFe_2O_4$/PANI-MWCNTs$_{1:20}$ (40 wt.%) composites were observed by a FEI-TECNAI G2 transmission electron microscopeoperating at 200 KV, TEM (FEI company). Elemental composition data was collected by Energy dispersive X-ray (EDX) performed using a TECNAI G2 microscope. The crystal structure of the sample was examined by X-ray diffraction (XRD) which was performed on Rigaku D/max-2400 diffractometer, using Cu-Kα radiation as the X-ray source in the 2θ range of 10–90°. X-ray photoelectron spectroscopy (XPS) was recorded on a PHI-5702 instrument.

Electrochemical measurements

Electrochemical measurements were carried out in the electrochemical workstation (CHI 660E, shanghai chenhua) with a standard three-electrode system at room temperature. The three-electrode system used glassy carbon electrode (GCE) with 3 mm diameter (catalyst loading 0.285 mg cm^{-2}) as working electrode, a platinum wire as the counter electrode and an Ag/AgCl (3 M KCl) electrode as the reference. The working electrode was polished mechanically with Al_2O_3 powders (Aldrich, 0.05 mm) and then cleaned with ethanol and deionized water, respectively. The catalyst ink was formed with 4 mg catalysts and 30 μL Nafion solutions (0.5 wt.%) dispersed in 1 mL water-ethanol solution with volume ratio of 1:1, followed by sonicating for at least 30 min. Then, 5 μL well-dispersed suspension (containing 20 μg catalyst) was loaded onto working electrode and dried at room temperature. The working electrodes were scanned several times until the signals were stabilized and then data were collected.

The electrolyte was 1 M KOH solution prepared from deionized water. Linear sweep voltammetry (LSV) worked from 0 to 1.0 V *vs*. Ag/AgCl at a scan rate of 5 mV s^{-1} in a N_2-saturated electrolyte. The electrochemical impedance spectroscopy (EIS) measurements were carried out in the same configuration at 0.50 V *vs*. Ag/AgCl from 10^5 to 0.01 Hz with an AC voltage of 5 mV. The durability test for OER was performed on the catalysts by cycling the electrode potential between 0 and 0.8 V *vs*. Ag/AgCl at 200 mV s^{-1} for 1000 cycles, after which the polarization curves for the OER was measured. The electrical double layer capacitor (C_{dl}) were measured from double-layer charging curves using cyclic voltammograms(CVs) in a small potential range of 1.22–1.28 V *vs*. RHE at different scan rates (2–10 mV s^{-1}). Working electrodes were scanned for several potential cycles until the signals were stabilized, and then the CV data were collected. The plot of current density (at 1.25 V *vs*. RHE) against scan rate has a linear relationship and its slope is the C_{dl}. The current density was normalized to the geometrical surface area. All the potentials reported in our work were against reversible hydrogen electrode (RHE) through RHE calibration. For conversion of the obtained potential (*vs*. Ag/AgCl) to RHE, eq 1 was used [37].

$$E_{RHE} = E_{Ag\,|\,AgCl} + 0.197 + 0.059 \times pH \quad (1)$$

Result and discussion

Fig. 1A illustrates the morphologies of MWCNTs, we can obviously observe that the surface of the nanotubes is smooth. However, there is an amorphous component wrapping the outside of the tube perimeter in Fig. 1B, demonstrating that the PANI is successfully covered on MWCNTs. Fig. 1C-D shows TEM micrographs of $CoFe_2O_4$/MWCNTs (40 wt.%) hybrid and $CoFe_2O_4$/PANI-MWCNTs $_{1:20}$ (40 wt.%) hybrid. On the bare MWCNTs support, $CoFe_2O_4$ metal particles prone to cluster, but when supported on MWCNTs with PANI functionalization, $CoFe_2O_4$ NPs are more evenly separated and well dispersed in the range of 3.28-10.59 nm with an average particle size of 6.22 nm. The Scanning electron microscopy (SEM) and TEM images of $CoFe_2O_4$/PANI-MWCNTs$_{1:20}$ (20 wt.%, 30 wt.%, 50 wt.%, and 60 wt.%) are also providied in Fig. S1. The EDX pattern in the insert of Fig. 1F reveals that Co, Fe, C, O and N are main elements and Cu element arising from copper grid is also detected. The existence of the N element further indicates that the MWCNTs have been functionalized by PANI. Fig. 1G-

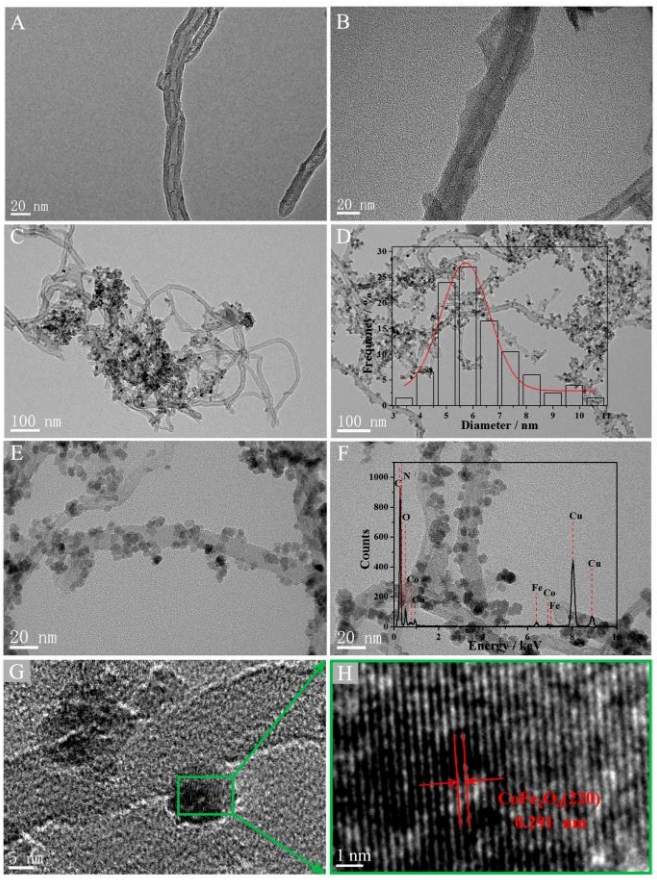

Fig.1 TEM images of (A) MWCNTs; (B) PANI-MWCNTs$_{1:20}$; (C) $CoFe_2O_4$/MWCNTs (40 wt.%); (D-F) $CoFe_2O_4$/PANI-MWCNTs$_{1:20}$ (40 wt.%); and HRTEM (G,H) images of

$CoFe_2O_4$/PANI-MWCNTs$_{1:20}$ (40 wt.%). The inset of TEM image (D) is size distribution histograms; and the inset of TEM image (F) is EDX pattern.

H show high-resolution transmission electron microscopy (HRTEM) images of the catalyst samples. The lattice planes with an interlayer distance of 0.291 nm correspond to $CoFe_2O_4$ (220) crystal planes.

The X-ray diffraction (XRD) patterns of samples are shown in Fig. 2A. The diffraction peaks at 26.0°, 43.2° are assigned to (002) and (100) planes of hexagonal graphite. And the appearance of these peaks with high intensity suggests that MWCNTs have a high graphitic structure. For PANI-MWCNTs, the diffraction peaks with lower intensity are similar to MWCNTs, which indicates that an extremely thin PANI film is covered on the MWCNTs [29, 38]. The XRD patterns of $CoFe_2O_4$/PANI-MWCNTs$_{1:20}$ (40 wt.%) hybrid at 2θ = 18.4°, 30.2°, 35.4°, 42.9°, 56.9° and 62.4° correspond to (111), (220), (311), (400), (511) and (440) crystal planes of $CoFe_2O_4$ (PDF#22-1086), while the peak at around 26° is attributed to (002) planes of MWCNTs. The results of XRD patterns prove that the $CoFe_2O_4$ NPs are efficiently immobilized on PANI-MWCNTs and have a highly crystalline fcc phase.

To obtain the oxidation state and the surface chemical composition of $CoFe_2O_4$/PANI-MWCNTs$_{1:20}$ (40 wt.%) hybrid, X-ray photoelectron spectroscopy (XPS) measurements are the composite in the Co 2p region is shown in Fig. 2C. It can be deconvoluted into four peaks. The peaks with binding energies (BE) of about 780.4 and 786.1 eV are in accord with Co $2p_{3/2}$ and its shakeup satellites, while the higher BE peaks around 796.1 and 802.7 eV correspond to Co $2p_{1/2}$ and its shakeup satellites, respectively. The existence of Co $2p_{3/2}$ and Co $2p_{1/2}$ main peaks and shake-up satellite peaks indicates the presence of Co^{2+} in the high-spin state [39]. For the high-resolution XPS spectrum of Fe 2p (Fig. 2D), all the deconvoluted Fe 2p spectra generally show two main peaks for Fe $2p_{3/2}$ and Fe $2p_{1/2}$ at a BE of around 710.7 and 724.2 eV, and Fe $2p_{3/2}$ accompanied by a satellite line visible at a BE of around 718.3 eV, only indicative of the presence of Fe^{3+} cations [39, 40]. Meanwhile, the presence of the peak around 713.3 eV implies that the Fe^{3+} species exist in more than one coordination environment. This could ascribe to the high affinity of Co^{2+} ions in octahedral sites of inverse spinel structure [41], demonstrating the existence of $CoFe_2O_4$. According to the C 1s XPS spectra of the catalyst as shown in Fig. 2E, the peaks at 284.6, 285.2, 286.6, 288.7 and 290.6 eV corresponding to the oxygen and carbon atoms in the forms C=C, C–N, C–O, C=O and O-C=O, respectively [42, 43]. Fig. 2F displays the XPS spectrum of N 1s, which is composed of three peaks at about 398.8 eV (=N–), 400.0 eV (–NH–), and 401.2 eV ($–N^+–$), which indicates the acid-treatment MWCNTs were successfully decorated by PANI [29]. The highest BE peak observed in N^+ is due to the protonated amine units.

The electrochemical activity of the support materials for OER has been evaluated with polarization curves. The polarization curves for a series of MWCNTs which are decorated with different mass ratios of PANI are measured in N_2-saturated 1M KOH solution with a scan rate of 5 mV s^{-1} at room temperature. It is well-known that MWCNTs is a poor OER catalyst with a slight current density. However, decorating MWCNTs with PANI can promote the electrochemical activity. As is shown in Fig. 3, PANI-MWCNTs$_{1:20}$ hybrid is considered as the best support material for OER due to the most negative onset potential and highest current density. Meanwhile, other

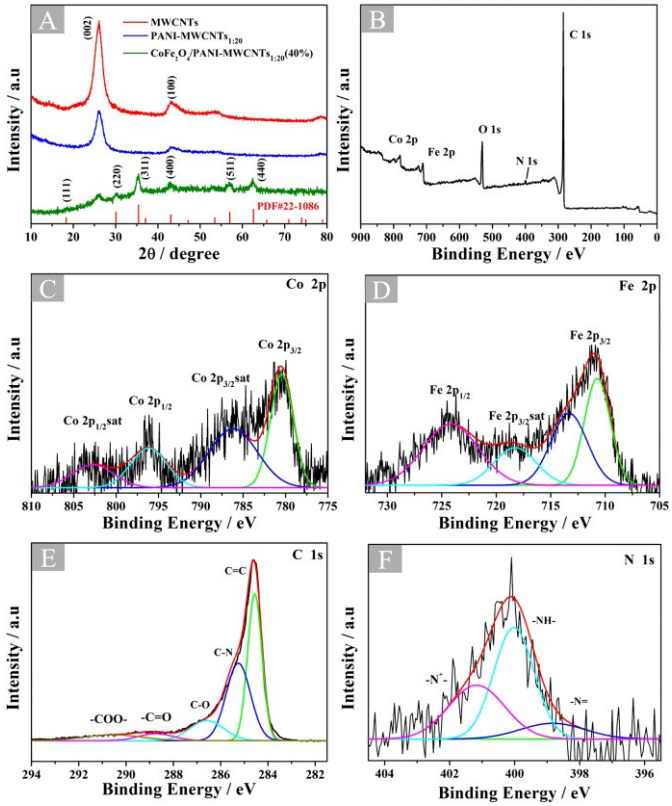

Fig.2 (A) XRD patterns of MWCNTs, PANI-MWCNTs, $CoFe_2O_4$/PANI-MWCNTs$_{1:20}$ (40 wt.%); Typical (B) XPS survey spectrum, deconvoluted (C) Co 2p spectrum, (D) Fe 2p spectrum, (E) C 1s spectrum and (F) N 1s spectrum of $CoFe_2O_4$/PANI-MWCNTs$_{1:20}$ (40 wt.%) composites.

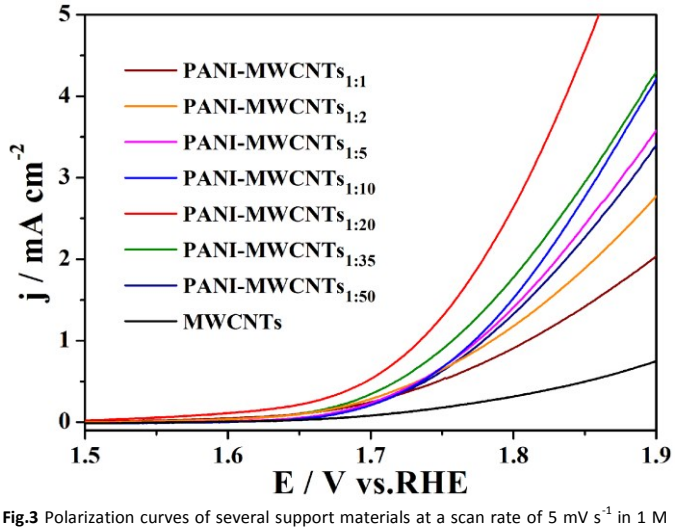

Fig.3 Polarization curves of several support materials at a scan rate of 5 mV s^{-1} in 1 M KOH.

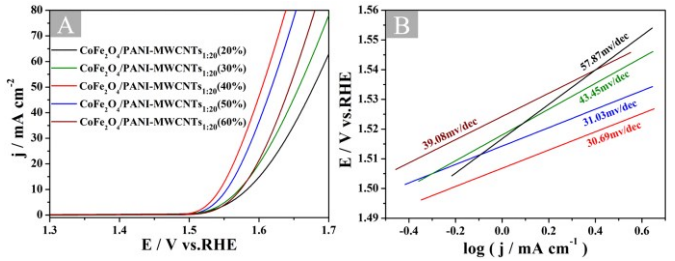

Fig.4 (A) Polarization curves obtained with several catalysts as indicated and (B) corresponding Tafel plots recorded on GCE with a catalyst loading of 0.28 mg cm^{-2}.

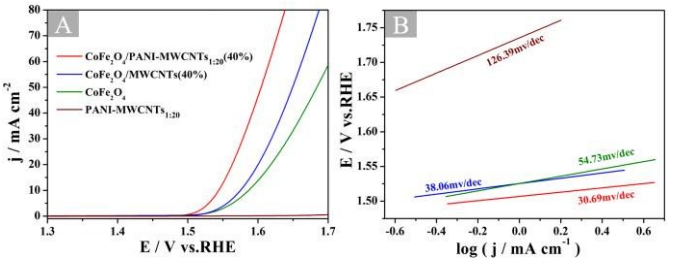

Fig.5 (a) polarization curves obtained with several catalysts as indicated and (b) corresponding Tafel plots recorded on GCE with a catalyst loading of 0.28 mg cm^{-2}.

PANI–MWCNTs hybrids also exhibit better OER catalytic activity than pure MWCNTs, assuring that the PANI-MWCNTs material has a high effective surface area which is beneficial for electronic transmission. Generally speaking, MWCNTs functionalized with PANI is available for promoting synergistically the OER.

According to the polarization curves in Fig. 4A, the PANI-$MWCNTs_{1:20}$ hybrid with different loading amounts of $CoFe_2O_4$ is evaluated in the same condition. The contents of $CoFe_2O_4$ on the PANI-$MWCNTs_{1:20}$ is identified by atomic absorption spectroscopy (AAS) as 18.95 wt.%, 28.14 wt.%, 38.78 wt.%, 47.33 wt.% and 58.64 wt.%, which are close to theoretical value (Table S3). As we all know, the overpotential for different catalysts to deliver a 10.0 mA cm^{-2} current density is a metric related to solar fuel synthesis [44, 45]. The overpotential at a current density of 10.0 mA cm^{-2} of these $CoFe_2O_4$/PANI-$MWCNTs_{1:20}$ samples with various $CoFe_2O_4$ loadings (20 wt.%, 30 wt.%, 40 wt.%, 50 wt.% and 60 wt.%) are estimated to be 353, 342, 314, 324 and 344 mV, respectively, which show a volcanic type trending. With the increase of $CoFe_2O_4$ content, the OER activity increases firstly and reaches the maximum value when the $CoFe_2O_4$ content is 40 wt.%. Then it declines sharply, indicating that the synergistic effect is not apparent when the loading amount of $CoFe_2O_4$ is too low or too high. Meanwhile, the Tafel plots of these catalysts which derive from the polarization curves fit well with the Tafel equation [$\eta = a + b\log(j)$, where η is the over-potential, b is the Tafel slope and j is the current density] at different overpotential ranges, and only the linear portions were selected to obtain a clear comparison. As is shown in Fig. 5B, the Tafel slopes of all the catalysts are between ~30.69 and ~57.87 mV dec^{-1}. A smaller Tafel slope means a faster increase of the OER rate with increasing potential [46]. Above all, $CoFe_2O_4$/PANI-$MWCNTs_{1:20}$ (40 wt.%) hybrid is the relatively optimal electrocatalyst for its low overpotential (314 mV) and small Tafel slope (~30.69 mV dec^{-1}). Furthermore, a detailed comparison of different highly active spinel-type OER catalysts was shown in Table S4, and further confirming the outstanding catalytic behavior of $CoFe_2O_4$/PANI-$MWCNTs_{1:20}$ (40 wt.%) hybrid.

Moreover, the catalytic activity of $CoFe_2O_4$/PANI-$MWCNTs_{1:20}$ (40 wt.%) hybrid is compared with $CoFe_2O_4$/MWCNTs (40 wt.%) hybrid, pure $CoFe_2O_4$ NPs and PANI-MWCNTs in the same condition. As is shown in Fig. 5, PANI-MWCNTs hybrid possesses relatively negligible catalytic activity due to the low current density and high Tafelslope (126.39 mV dec^{-1}). The OER onset potential of the $CoFe_2O_4$/PANI-$MWCNTs_{1:20}$ (40 wt.%) hybrid is about 1.50 V (*vs.* RHE) in 1 M KOH (an overpotential only about 270 mV, at pH 13.6), which is much more negative than that of the $CoFe_2O_4$/MWCNTs (40 wt.%) composite and pure $CoFe_2O_4$ NPs electrodes. Particularly, The Tafel slope of $CoFe_2O_4$/PANI-$MWCNTs_{1:20}$ (40 wt.%) hybrid (~30.69 mV dec^{-1}) is much smaller than those of $CoFe_2O_4$/MWCNTs (40 wt.%) hybrid (~38.06 mV dec^{-1}) and pure $CoFe_2O_4$ NPs (~54.73 mV dec^{-1}). The results strongly demonstrate that the $CoFe_2O_4$/PANI-$MWCNTs_{1:20}$ (40 wt.%) hybrid has excellent OER catalytic activities in alkaline solution in comparison to pure $CoFe_2O_4$ NPs and $CoFe_2O_4$/MWCNTs (40 wt.%) hybrid. This is probably contributed to PANI which could promote the synergistic effect between $CoFe_2O_4$ NPs and MWCNTs components.

In addition, by comparing $CoFe_2O_4$/PANI-$MWCNTs_{1:20}$ (40 wt.%) hybrid with commercial IrO_2 and RuO_2 in Fig. S2, the catalyst yielded lower overpotential at current density of 10 mA cm^{-2}, whereas it dispalyed higher overpotential at current density of 20 mA cm^{-2} for IrO_2 and 50 mA cm^{-2} for RuO_2. As

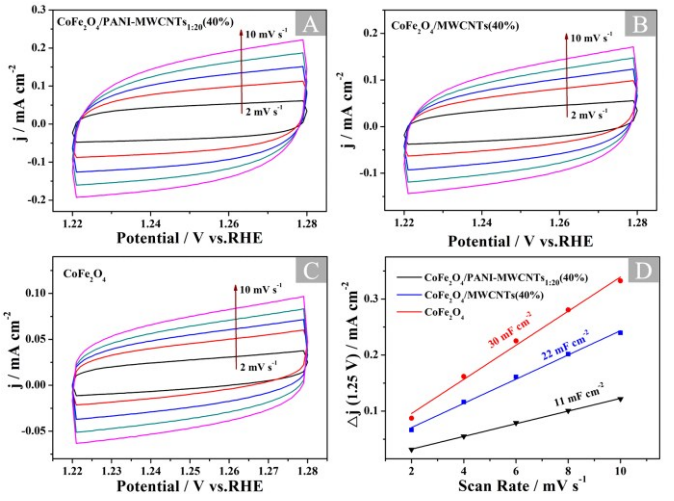

Fig.6 Voltammograms of the (A) $CoFe_2O_4$/PANI-$MWCNTs_{1:20}$ (40 wt.%), (B) $CoFe_2O_4$/MWCNTs (40 wt.%) and (C) $CoFe_2O_4$ NPs at various scan rates (2–10 mV s^{-1}) used to (D) estimate the C_{dl} and relative electrochemically active surface area.

also observed, the Tafel slope of the catalyst is much lower than IrO_2 (62.50 mV dec^{-1}) and RuO_2 (91.89 mV dec^{-1}).

We also estimated the electrochemically active surface area by the electrochemical double-layer capacitances (C_{dl}) using a simple cyclic voltammetry (CV) method. Current response in the potential window used for the CV (1.22–1.28 V *vs*. RHE) at different scan rates (2–10 mV s^{-1}) should be due only to the charging of the double-layer (Fig. 6A, B and C). The C_{dl} for each sample, which should be directly proportional to the surface area, are extracted by plotting the $\Delta j = j_a - j_c$ at a given potential (1.25 V *vs*. RHE) against the CV scan rates (Fig. 6D) [47, 48]. By calculating the slope from the linear relationship of the current density against the scan rate, C_{dl} of the $CoFe_2O_4$/PANI-$MWCNTs_{1:20}$ (40 wt.%) hybrid is confirmed to be ~30 mF cm^{-2}, which is much higher than that of $CoFe_2O_4$/MWCNTs (40 wt.%) hybrid (~22 mF cm^{-2}) and pure $CoFe_2O_4$ NPs (~11 mF cm^{-2}). The results demostrated that the $CoFe_2O_4$/PANI-$MWCNTs_{1:20}$ (40 wt.%) hybrid has relatively larger active surface area. Meanwhile, this increase in C_{dl} indicates better exposure and enhanced utilization of electroactive sites, which certainly ascribe to the introduction of PANI and contribute to the improved catalytic performance.

Additionally, we used electrochemical impedance spectroscopy (EIS) to investigate the electrode kinetics under the catalytic OER operating conditions. The EIS data of $CoFe_2O_4$/PANI-$MWCNTs_{1:20}$ (40 wt.%) hybrid, $CoFe_2O_4$/MWCNTs (40 wt.%) hybrid and pure $CoFe_2O_4$ NPs have been detailed recorded at an operating potential of 0.50 V *vs*. Ag/AgCl in Fig.7A. It is revealed that the $CoFe_2O_4$/PANI-$MWCNTs_{1:20}$ (40 wt.%) hybrid shows a much smaller radius of the semicircle in the Nyquist plots compared with $CoFe_2O_4$/MWCNTs (40 wt.%) hybrid and pure $CoFe_2O_4$ NPs, indicating that the reaction sites of the electrode increased, which leads to facile transfer of charge species (electron and ions OH^-). The reason can be attribute to the presence of the PANI, which makes the $CoFe_2O_4$ NPs attach to MWCNTs closely. Also, the smaller Tafel slope and lower resistance correspond to a more favorable OER kinetics of the $CoFe_2O_4$/PANI-$MWCNTs_{1:20}$ (40 wt.%) hybrid.

The stabilities of catalysts for the OER were appraised with the chronoamperometric method in Fig. 7B. It can be observed that the Current-time (i–t) curves of the $CoFe_2O_4$/PANI-$MWCNTs_{1:20}$ (40 wt.%) hybrid worked at a potential of 0.54 V (*vs*. Ag/AgCl) for at least 40 h. In the initial period, the decay current density decreases rapidly. However, during the whole time, the larger residual current is nearly constant. Furthermore, the durability test was also carried out by cycling catalyst continuously for 1000 cycles (the inset of Fig. 7B). At the end of the cycling, it afforded similar i-V curves as initial test, demonstrating the high stability of $CoFe_2O_4$/PANI-$MWCNTs_{1:20}$ (40 wt.%) in alkaline. Moreover, the stability of the $CoFe_2O_4$/PANI-$MWCNTs_{1:20}$ (40 wt.%) hybrid has been compared with $CoFe_2O_4$/MWCNTs (40 wt.%) hybrid by i–t curves at the same condition in Fig. S3. Obviously, the $CoFe_2O_4$/PANI-$MWCNTs_{1:20}$ (40 wt.%) hybrid has higer current density, indicating that the introduction of PANI to this electrocatalyst could improve the synergistic effect between $CoFe_2O_4$ NPs and MWCNTs to promote stability of the catalyst.

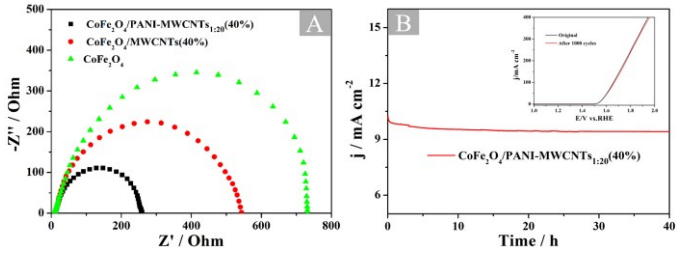

Fig.7 (A) Nyquist plots of $CoFe_2O_4$/PANI-$MWCNTs_{1:20}$ (40 wt.%), $CoFe_2O_4$/MWCNTs (40 wt.%) and $CoFe_2O_4$ are recorded at the over-potential of 0.50 V (*vs.* Ag/AgCl); (B) Chronoamperometric measurement in N_2-saturated 0.1 M KOH at 0.54 V (*vs.* Ag/AgCl) (inset: polarization curves of $CoFe_2O_4$/PANI-$MWCNTs_{1:20}$ (40 wt.%) before and after 1000 cycles).

Conclusion

In conlusion, we have developed a novel in-situ synthetic method to prepare $CoFe_2O_4$ NPs on the as-prepared polyaniline-multiwalled carbon nanotubes at mild temperature (120 °C) and room atmosphere. The mass ratios of PANI-MWCNTs and the loading amounts of $CoFe_2O_4$ are explored in this paper. Our study shows that the introduction of PANI could improve the synergistic effect between $CoFe_2O_4$ NPs and MWCNTs, so as to promote the electrical conductivity and stability of the catalyst. Meanwhile, PANI provides more active sites to result in a homogeneous distribution of $CoFe_2O_4$ NPs. The OER activities of the $CoFe_2O_4$/PANI-$MWCNTs_{1:20}$ (40 wt.%) hybrid were further compared with the $CoFe_2O_4$/MWCNTs (40 wt.%) and pure $CoFe_2O_4$ NPs. By comparison, we found that the $CoFe_2O_4$/PANI-$MWCNTs_{1:20}$ (40 wt.%) hybrid exhibits the most superior oxygen evolution activity and strong durability as a promising alternative to noble metal catalysts in OER. It is believed that this simple preparation method paved a possible way to fabricate a range of spinel-type oxide/PANI-MWCNTs based composite as an outstanding OER electrocatalyst.

Notes and References

1 J. L. Dempsey, B. S. Brunschwig, J. R. Winkler and H. B. Gray, *Accounts Chem. Res.*, 2009, **42**, 1995-2004.
2 J. Li, P. Zhou, F. Li, R. Ren, Y. Liu, J. Niu, J. Ma, X. Zhang, M. Tian, J. Jin and J. Ma, *J. Mater. Chem. A*, 2015, **3**, 11261-11268.
3 F. Li, L. Zhang, J. Li, X. Lin, X. Li, Y. Fang, J. Huang, W. Li, M. Tian, J. Jin and R. Li, *J. Power Sources*, 2015, **292**, 15-22.
4 M. Gong, W. Zhou, M.-C. Tsai, J. Zhou, M. Guan, M.-C. Lin, B. Zhang, Y. Hu, D.-Y. Wang, J. Yang, S. J. Pennycook, B.-J. Hwang and H. Dai, *Nat. Commun.*, 2014, **5**, 4695-4701.
5 C. G. Morales-Guio, L. A. Stern and X. Hu, *Chem. Soc. Rev.*, 2014, **43**, 6555-6569.
6 J. Landon, E. Demeter, N. İnoğlu, C. Keturakis, I. E. Wachs, R. Vasić, A. I. Frenkel and J. R. Kitchin, *ACS Catal*, 2012, **2**, 1793-1801.
7 Z. Zhuang, W. Sheng and Y. Yan, *Adv. Mater.*, 2014, **26**, 3950-3955.

8 A. Kargar, S. Yavuz, T. K. Kim, C. H. Liu, C. Kuru, C. S. Rustomji, S. Jin and P. R. Bandaru, *ACS Appl. Mater. Interfaces*, 2015, **23**, 17851-17856.
9 H. Wang, Z. Li, G. Li, F. Peng and H. Yu, *Cataly. Today*, 2015, **245**, 74-78.
10 Y. Fang, X. Li, Y. Hu, F. Li, X. Lin, M. Tian, X. An, Y. Fu, J. Jin and J. Ma, *J. Power Sources*, 2015, **300**, 285-293.
11 V. Petrykin, K. Macounova, O. A. Shlyakhtin and P. Krtil, *Angew. Chem. Int. Ed.*, 2010, **49**, 4813-4815.
12 V. 8-Petrykin, K. Macounova, O. Shlyakhtin and P. Krtil, *Angew. Chem. Int. Ed.*, 2010, **122**, 4923-4925.
13 Y. Xu, W. Bian, J. Wu, J.-H. Tian and R. Yang, *Electrochim. Acta*, 2015, **151**, 276-283.
14 Y. Liang, Y. Li, H. Wang, J. Zhou, J. Wang, T. Regier and H. Dai, *Nat. Mater.*, 2011, **10**, 780-786.
15 L. Trotochaud, J. K. Ranney, K. N. Williams and S. W. Boettcher, *J. Am. Chem. Soc.*, 2012, **134**, 17253-17261.
16 Y. Liang, Y. Li, H. Wang, J. Zhou, J. Wang, T. Regier and H. Dai, *Nat. Mater.*, 2011, **10**, 780-786.
17 J. Geng, L. Kuai, E. Kan, Q. Wang and B. Geng, *ChemSusChem*, 2015, **8**, 659-664.
18 T. N. Lambert, J. A. Vigil, S. E. White, D. J. Davis, S. J. Limmer, P. D. Burton, E. N. Coker, T. E. Beechem and M. T. Brumbach, *Chem. Commun*., 2015, **51**, 9511-9514.
19 D. Zhang, L. Meng, J. Shi, N. Wang, S. Liu and C. Li, *Electrochim. Acta*, 2015, **169**, 402-408.
20 F. Cheng, J. Shen, B. Peng, Y. Pan, Z. Tao and J. Chen, *Nat. Chem.*, 2011, **3**, 79-84.
21 J. Li, M. Zou, W. Wen, Y. Zhao, Y. Lin, L. Chen, H. Lai, L. Guan and Z. Huang, *J. Mater. Chem. A*, 2014, 2, 10257-10262.
22 H. Zhu, S. Zhang, Y.-X. Huang, L. Wu and S. Sun, *Nano Lett.*, 2013, **13**, 2947-2951.
23 M. Li, Y. Xiong, X. Liu, X. Bo, Y. Zhang, C. Han and L. Guo, *Nanoscale*, 2015, **7**, 8920-8930.
24 W. Bian, Z. Yang, P. Strasser and R. Yang, *J. Power Sources*, 2014, **250**, 196-203.
25 S. Liu, W. Bian, Z. Yang, J. Tian, C. Jin, M. Shen, Z. Zhou and R. Yang, *J. Mater. Chem. A*, 2014, **2**, 18012-18017.
26 Y.-X. Zhang, X. Guo, X. Zhai, Y.-M. Yan and K.-N. Sun, *J. Mater. Chem. A*, 2015, **3**, 1761-1768.
27 T.-H. Hu, Z.-S. Yin, J.-W. Guo and C. Wang, *J. Power Sources*, 2014, **272**, 661-671.
28 H. Y. Lee, W. Vogel and P. P. Chu, *Langmuir*, 2011, **27**, 14654-14661.
29 L. Shi, R.-P. Liang and J.-D. Qiu, *J. Mater. Chem*, 2012, **22**, 17196-17203.
30 S. Chen, Z. Wei, X. Qi, L. Dong, Y. G. Guo, L. Wan, Z. Shao and L. Li, *J. Am. Chem. Soc.*, 2012, **134**, 13252-13255.
31 M. R. Nabid, Y. Bide, N. Ghalavand and M. Niknezhad, *Appl. Organomet. Chem.*, 2014, **28**, 389-395.
32 J. Armijo, Oxid. Met., 1969, **1**, 171-198.
33 D. P. Dubal, P. Gomez-Romero, B. R. Sankapal and R. Holze, *Nano Energy*, 2015, **11**, 377-399.
34 M. U. Anu Prathap and R. Srivastava, *Nano Energy*, 2013, **2**, 1046-1053.
35 K. Kalpanadevi, C. R. Sinduja and R. Manimekalai, *Mater. Sci-Poland*, 2014, **32**, 34-38.
36 P. Zamani, D. Higgins, F. Hassan, G. Jiang, J. Wu, S. Abureden and Z. Chen, *Electrochim. Acta*, 2014, **139**, 111-116.
37 X. Lu, W.-L. Yim, B. H. Suryanto and C. Zhao, *J. Am. Chem. Soc.*, 2015, **137**, 2901-2907.
38 G. Nie, L. Zhang and Y. Cui, *Reac. Kinet. Mech. Cat.*, 2012, **108**, 193-204.
39 H. L. Yuan, Y. Q. Wang, S. M. Zhou, L. S. Liu, X. L. Chen, S. Y. Lou, R. J. Yuan, Y. M. Hao and N. Li, *Nanoscale Res. Lett.*, 2010, **5**, 1817-1821.
40 H. Kim, D.-H. Seo, H. Kim, I. Park, J. Hong, K.-Y. Park and K. Kang, *Chem. Mater.*, 2012, **24**, 720-725.
41 Z. Gu, X. Xiang, G. Fan and F. Li, *J. Phys. Chem. C*, 2008, **112**, 18459-18466.
42 P. Xiong, H. Huang and X. Wang, *J. Power Sources*, 2014, **245**, 937-946.
43 S. Abdulla, T. L. Mathew and B. Pullithadathil, *Sens Actuators B Chem*, 2015, **221**, 1523-1534.
44 L. Wu, Q. Li, C. H. Wu, H. Zhu, A. Mendoza-Garcia, B. Shen, J. Guo and S. Sun, *J. Am. Chem. Soc.*, 2015, **137**, 7071-7074.
45 C. C. McCrory, S. Jung, J. C. Peters and T. F. Jaramillo, *J. Am. Chem. Soc.*, 2013, **135**, 16977-16987.
46 Z. Wang, S. Xiao, Z. Zhu, X. Long, X. Zheng, X. Lu and S. Yang, *ACS Appl. Mater. Interfaces*, 2015, **7**, 4048-4055.
47 K. Wang, H. Wu, Y. Meng and Z. Wei, *Small*, 2014, 10, 14-31.
48 K. Gong, F. Du, Z. Xia, M. Durstock and L. Dai, *Science*, 2009, **323**, 760-764.

A Facile preparation of $CoFe_2O_4$ nanoparticles on Polyaniline-Functioned Carbon Nanotubes as Enhanced Catalysts for Oxygen Evolution Reaction

Yang Liu, Jing Li, Feng Li, Wenzhu Li, Haidong Yang, Xueyao Zhang, Yansheng Liu and Jiantai Ma*